

Highly sensitive UVA and violet photodetector based on single-layer graphene-TiO₂ heterojunction

FENG-XIA LIANG,¹ DENG-YUE ZHANG,¹ JIU-ZHEN WANG,¹ WEI-YU KONG,² ZHI-XIANG ZHANG,² YI WANG,² AND LIN-BAO LUO^{2,*}

¹*School of Materials Science and Engineering, Hefei University of Technology, Hefei Anhui 230009, China*

²*School of Electronic Science and Applied Physics, Hefei University of Technology, Hefei, Anhui 230009, China*

*luolb@hfut.edu.cn

Abstract: A highly sensitive ultraviolet A (UVA) and violet photodetector based on p-type single-layer graphene (SLG)-TiO₂ heterostructure was fabricated by transferring chemical vapor deposition derived SLG on the surface of commercial single-crystal TiO₂ wafer. Optoelectronic analysis reveals the as-fabricated Schottky junction PD was highly sensitive to light illumination in UVA and violet range, with peak sensitivity at 410 nm and excellent stability and reproducibility, but virtually blind to illumination with wavelength less than 350 nm or more than 460 nm. The on/off ratio of the device was calculated to be 6.8×10^4 , which is better than the majority of previously reported TiO₂ based PDs. What is more, the rise/fall time were estimated to be 0.74/1.18 ms, much faster than other TiO₂ based counterparts. The totality of the above result signifies that the present SLG-TiO₂ Schottky junction photodetector may have promising application in future high-speed, high-sensitivity optoelectronic nanodevices and systems.

© 2016 Optical Society of America

OCIS codes: (260.7190) Ultraviolet; (230.5160) Photodetectors; (160.4760) Optical properties; (160.5335) Photosensitive materials; (250.6715) Switching.

References and links

1. X. Yu, Z. Zhao, J. Zhang, W. Guo, J. Qiu, D. Li, Z. Li, X. Mou, L. Li, A. Li, and H. Liu, "Rutile nanorod/anatase nanowire junction array as both sensor and power supplier for high-performance, self-Powered, wireless UV photodetector," *Small* **12**(20), 2759–2767 (2016).
2. M. Peng, Y. Liu, A. Yu, Y. Zhang, C. Liu, J. Liu, W. Wu, K. Zhang, X. Shi, J. Kou, J. Zhai, and Z. L. Wang, "Flexible self-powered GaN ultraviolet photoswitch with piezo-phototronic effect enhanced on/off ratio," *ACS Nano* **10**(1), 1572–1579 (2016).
3. Q. Wang, J. J. Li, and C. Z. Gu, "Enhanced UV response of single anodic TiO₂ nanotube: effect of water-modified microstructures," *J. Phys. Chem. C* **116**(32), 16864–16869 (2012).
4. Y. Han, G. Wu, H. Li, M. Wang, and H. Chen, "Highly efficient ultraviolet photodetectors based on TiO₂ nanocrystal-polymer composites via wet processing," *Nanotechnology* **21**(18), 185708 (2010).
5. L. B. Wang, W. Y. Yang, H. N. Chong, L. Wang, F. M. Gao, L. H. Tian, and Z. B. Yang, "Efficient ultraviolet photodetectors based on TiO₂ nanotube arrays with tailored structures," *RSC Advances* **5**(65), 52388–52394 (2015).
6. H. L. Xue, X. Z. Kong, Z. R. Liu, C. X. Liu, J. R. Zhou, W. Y. Chen, S. P. Ruan, and Q. Xu, "TiO₂ based metal-semiconductor-metal ultraviolet photodetectors," *Appl. Phys. Lett.* **90**(20), 201118 (2007).
7. D. I. Son, H. Y. Yang, T. W. Kim, and W. I. Park, "Photoresponse mechanisms of ultraviolet photodetectors based on colloidal ZnO quantum dot-graphene nanocomposites," *Appl. Phys. Lett.* **102**(2), 021105 (2013).
8. Y. Liang, H. Liang, X. D. Xiao, and S. K. Hark, "The epitaxial growth of ZnS nanowire arrays and their applications in UV-light detection," *J. Mater. Chem.* **22**(3), 1199–1205 (2012).
9. K. Zheng, F. Meng, L. Jiang, Q. Yan, H. H. Hng, and X. Chen, "Visible photoresponse of single-layer graphene decorated with TiO₂ nanoparticles," *Small* **9**(12), 2076–2080 (2013).
10. Y. Xie, L. Wei, G. Wei, Q. Li, D. Wang, Y. Chen, S. Yan, G. Liu, L. Mei, and J. Jiao, "A self-powered UV photodetector based on TiO₂ nanorod arrays," *Nanoscale Res. Lett.* **8**(1), 188 (2013).
11. E. Hosono, S. Fujihara, K. Kakiuchi, and H. Imai, "Growth of submicrometer-scale rectangular parallelepiped rutile TiO₂ films in aqueous TiCl₃ solutions under hydrothermal conditions," *J. Am. Chem. Soc.* **126**(25), 7790–7791 (2004).

12. C. Lee, X. Wei, J. W. Kysar, and J. Hone, "Measurement of the elastic properties and intrinsic strength of monolayer graphene," *Science* **321**(5887), 385–388 (2008).
13. K. S. Kim, Y. Zhao, H. Jang, S. Y. Lee, J. M. Kim, K. S. Kim, J. H. Ahn, P. Kim, J. Y. Choi, and B. H. Hong, "Large-scale pattern growth of graphene films for stretchable transparent electrodes," *Nature* **457**(7230), 706–710 (2009).
14. X. Li, Y. Zhu, W. Cai, M. Borysiak, B. Han, D. Chen, R. D. Piner, L. Colombo, and R. S. Ruoff, "Transfer of large-area graphene films for high-performance transparent conductive electrodes," *Nano Lett.* **9**(12), 4359–4363 (2009).
15. X. Li, H. Zhu, K. Wang, A. Cao, J. Wei, C. Li, Y. Jia, Z. Li, X. Li, and D. Wu, "Graphene-on-silicon Schottky junction solar cells," *Adv. Mater.* **22**(25), 2743–2748 (2010).
16. G. Eda and M. Chhowalla, "Chemically derived graphene oxide: towards large-area thin-film electronics and optoelectronics," *Adv. Mater.* **22**(22), 2392–2415 (2010).
17. F. Lin, S. W. Chen, J. Meng, G. Tse, X. W. Fu, F. J. Xu, B. Shen, Z. M. Liao, and D. P. Yu, "Graphene/GaN diodes for ultraviolet and visible photodetectors," *Appl. Phys. Lett.* **105**(7), 073103 (2014).
18. T. Mueller, F. N. Xia, and P. Avouris, "Graphene photodetectors for high-speed optical communications," *Nat. Photonics* **4**(5), 297–301 (2010).
19. X. W. Fu, Z. M. Liao, Y. B. Zhou, H. C. Wu, Y. Q. Bie, J. Xu, and D. P. Yu, "Graphene/ZnO nanowire/graphene vertical structure based fast-response ultraviolet photodetector," *Appl. Phys. Lett.* **100**(22), 223114 (2012).
20. B. Nie, J. G. Hu, L. B. Luo, C. Xie, L. H. Zeng, P. Lv, F. Z. Li, J. S. Jie, M. Feng, C. Y. Wu, Y. Q. Yu, and S. H. Yu, "Monolayer graphene film on ZnO nanorod array for high-performance Schottky junction ultraviolet photodetectors," *Small* **9**(17), 2872–2879 (2013).
21. J. Miao, W. Hu, N. Guo, Z. Lu, X. Liu, L. Liao, P. Chen, T. Jiang, S. Wu, J. C. Ho, L. Wang, X. Chen, and W. Lu, "High-responsivity graphene/InAs nanowire heterojunction near-infrared photodetectors with distinct photocurrent on/off ratios," *Small* **11**(8), 936–942 (2015).
22. L. Zeng, C. Xie, L. Tao, H. Long, C. Tang, Y. H. Tsang, and J. Jie, "Bilayer graphene based surface passivation enhanced nano structured self-powered near-infrared photodetector," *Opt. Express* **23**(4), 4839–4846 (2015).
23. A. I. Nusrir and M. O. Manasreh, "Self-powered near-infrared photodetector based on asymmetrical Schottky interdigital contacts," *IEEE Electron Device Lett.* **36**(11), 1172–1175 (2015).
24. Y. Wang, C. W. Ge, Y. F. Zou, R. Lu, K. Zheng, T. F. Zhang, Y.-Q. Yu, and L.-B. Luo, "Plasmonic indium nanoparticle-induced high-performance photoswitch for blue light detection," *Adv. Opt. Mater.* **4**(2), 291–296 (2016).
25. E. Enache-Pommer, B. Liu, and E. S. Aydil, "Electron transport and recombination in dye-sensitized solar cells made from single-crystal rutile TiO₂ nanowires," *Phys. Chem. Chem. Phys.* **11**(42), 9648–9652 (2009).
26. A. Kumar, A. R. Madaria, and C. W. Zhou, "Growth of aligned single-crystalline rutile TiO₂ nanowires on arbitrary substrates and their application in dye-sensitized solar cells," *J. Phys. Chem. C* **114**(17), 7787–7792 (2010).
27. Y. An, A. Behnam, E. Pop, and A. Ural, "Metal-semiconductor-metal photodetectors based on graphene/p-type silicon Schottky junctions," *Appl. Phys. Lett.* **102**(1), 013110 (2013).
28. S. Chand and S. Bala, "Analysis of current–voltage characteristics of inhomogeneous Schottky diodes at low temperatures," *Appl. Surf. Sci.* **252**(2), 358–363 (2005).
29. Y. Takanashi, N. Oyama, K. Momiyama, Y. Kimura, M. Niwano, and F. Hirose, "Alpha-sexthiophene/n-Si heterojunction diodes and solar cells investigated by I-V and C-V measurements," *Synth. Met.* **161**(23–24), 2792–2797 (2012).
30. L. B. Luo, J. J. Chen, M. Z. Wang, H. Hu, C. Y. Wu, Q. Li, L. Wang, J. A. Huang, and F. X. Liang, "Near-infrared light photovoltaic detector based on GaAs nanocone array/monolayer graphene Schottky junction," *Adv. Funct. Mater.* **24**(19), 2794–2800 (2014).
31. Y. L. Cao, Z. T. Liu, L. M. Chen, Y. B. Tang, L. B. Luo, J. S. Jie, W. J. Zhang, S. T. Lee, and C. S. Lee, "Single-crystalline ZnTe nanowires for application as high-performance green/ultraviolet photodetector," *Opt. Express* **19**(7), 6100–6108 (2011).
32. J. Miao, W. Hu, N. Guo, Z. Lu, X. Liu, L. Liao, P. Chen, T. Jiang, S. Wu, J. C. Ho, L. Wang, X. Chen, and W. Lu, "High-responsivity graphene/InAs nanowire heterojunction near-infrared photodetectors with distinct photocurrent on/off ratios," *Small* **11**(8), 936–942 (2015).
33. Y. Q. Yu, J. S. Jie, Q. Jiang, L. Wang, C. Y. Wu, Q. Peng, X. W. Zhang, Z. Wang, C. Xie, D. Wu, and Y. Jiang, "High-gain visible-blind UV photodetectors based on chlorine-doped n-type ZnS nanoribbons with tunable optoelectronic properties," *J. Mater. Chem.* **21**(34), 12632–12638 (2011).
34. C. Soci, A. Zhang, B. Xiang, S. A. Dayeh, D. P. R. Aplin, J. Park, X. Y. Bao, Y. H. Lo, and D. Wang, "ZnO nanowire UV photodetectors with high internal gain," *Nano Lett.* **7**(4), 1003–1009 (2007).
35. J. G. Ok, J. Y. Lee, H. W. Baac, S. H. Tawfick, L. J. Guo, and A. J. Hart, "Rapid anisotropic photoconductive response of ZnO-coated aligned carbon nanotube sheets," *ACS Appl. Mater. Interfaces* **6**(2), 874–881 (2014).
36. J. S. Jie, W. J. Zhang, Y. Jiang, X. M. Meng, Y. Q. Li, and S. T. Lee, "Photoconductive characteristics of single-crystal CdS nanoribbons," *Nano Lett.* **6**(9), 1887–1892 (2006).
37. L. B. Luo, L. H. Zeng, C. Xie, Y. Q. Yu, F. X. Liang, C. Y. Wu, L. Wang, and J. G. Hu, "Light trapping and surface plasmon enhanced high-performance NIR photodetector," *Sci. Rep.* **4**, 3914 (2014).

38. S. Bae, H. Kim, Y. Lee, X. Xu, J. S. Park, Y. Zheng, J. Balakrishnan, T. Lei, H. R. Kim, Y. I. Song, Y. J. Kim, K. S. Kim, B. Ozylmaz, J. H. Ahn, B. H. Hong, and S. Iijima, "Roll-to-roll production of 30-inch graphene films for transparent electrodes," *Nat. Nanotechnol.* **5**(8), 574–578 (2010).

1. Introduction

In recent years, ultraviolet photodetectors (UVPDs) have attracted wide research interest owing to their great potential in civilian and military applications including biological and chemical analysis, environmental monitoring, remote control and missile launch detection [1, 2]. UVPDs are generally fabricated from wide band-gap semiconductor materials which can strongly absorb light illumination in UV region. To date, various semiconductor materials such as TiO₂ [3–6], ZnO [7], and ZnS [8], have exhibited excellent UV light-absorption capabilities, and great potential for constructing high-performance UVPDs. Among these materials, titanium oxide (TiO₂) has received special research interest because of its excellent physical and optical properties, such as high melting point, chemical inertness, high photoconversion efficiency and photostability [9–11].

Graphene, as the most hotly-pursued material is structurally composed of a two dimensional of sp²-bonded carbon atoms with a one-atom thickness. It has been paid huge attention in the past decade because of its fascinating characteristics including high conductivity, good transparency, high carrier mobility, and electromechanical modulation [12–14]. By these tokens, graphene has become one of the most popular materials for application in various optoelectronic devices, e.g. solar cells, light-emitting diodes (LEDs) and photodetectors (PDs) [15–18]. As for PDs applications, researchers have successfully developed various high performance photodetectors based on graphene and other semiconductor materials (e.g. ZnO, InAs, and Ge) [19–22], which can take advantage of the synergistic effect of carrier transportation and light absorption. In addition, this type of SLG-semiconductor heterojunction devices were often characterized by a built-in electric field at the heterojunction interface, which is beneficial for efficient separation of the photo-generated electrons and holes, leading to good device performance in terms of high detectivity and fast response rate [23, 24]. Inspired by these concept, we herein report a graphene-single-crystal TiO₂ heterojunction PD for UVA and violet light illumination. The as-fabricated device exhibited obvious two advantageous features: (1) Relatively simple fabrication process. The present device only needs a transfer of CVD graphene on the TiO₂. Such a process is more convenient than the fabrication of other TiO₂ nanostructured based device which involves the synthesis of TiO₂ nanostructures using complicated instruments. (2) Good device reliability. Thanks to the precise control over device fabrication, the device performance of the as-fabricated PD is highly reproducible, leading to very good reproducibility and reliability [25, 26]. Device performance analysis reveals that the Schottky junction PD was highly sensitive to UVA and violet light illumination, with excellent stability and reproducibility, and fast response speed. In addition, it shows excellent spectral sensitivity, with peak sensitivity at 410 nm, but it was virtually blind to illumination with wavelength either less than 350 nm, or wavelength more than 460 nm. The on/off ratio of the device was calculated to be 6.8×10^4 , which is better than the majority of previously reported TiO₂ PDs.

2. Experimental section

2.1 Materials synthesis

The intrinsic single-crystal TiO₂ wafer (size of $10 \times 10 \times 0.5$ mm³, conductivity: 5×10^{-5} – 10^{-4} S/cm) with rutile phase was purchased from Hefei Kejing Materials Technology Co., LTD. The graphene film was synthesized through a chemical vapor deposition (CVD) approach that was performed in a tube furnace at a temperature of 1015 °C. During synthesis, Cu foil with a thickness of 50 μm, and a mixed gas composed of CH₄ (1 SCCM) and H₂ (99 SCCM) were used as catalytic substrate and reaction source, respectively. After deposition, the graphene film on Cu foils were deposited with polymethylmethacrylate (PMMA) solution

(5wt% in chlorobenzene) by spin-coating, and then soaked into a Marble's reagent solution (CuSO_4 : HCl : H_2O = 10 g: 50 ml: 50 ml) to remove the catalytic Cu substrate. To investigate the structures of the as-synthesized graphene, the graphene supported by PMMA was then transferred onto a $\text{SiO}_2/\text{n-Si}$ wafer and dried on a hot plate at 100 °C for at least 10 min., followed by removal of the PMMA in acetone solution. To achieve p-type conductivity, the as-deposited graphene was then treated in an HNO_3 solution for 5 minutes and then cleaned in distilled water. The Raman analysis of the graphene film was performed on a Raman Spectrometer (JY, LabRAM HR800).

2.2 Device Fabrication and Characterization

To assemble the p-type graphene- TiO_2 PDs, the commercial single crystal TiO_2 substrate was successively cleaned in an acetone, alcohol, and deionized water to remove possible contaminants and subsequently dried with nitrogen gas. The substrate which was partially pasted with sellotape was soaked in a deionized water, and then slowly lifted to mount the graphene thin film onto the exposed area of TiO_2 substrate. Afterwards, Ag paste was placed at both the Cu foil and the corner of the graphene film, serving as the electrode of the as-fabricated device. For the convenience of experiment, the as-prepared device was then mounted onto a printed circuit board (PCB). The electrical property of SLG- TiO_2 Schottky junction device was studied by using an I - V characterization system (Keithley Company, SCS-4200). To examine the spectral selectivity and response rate of the graphene- TiO_2 PD, a home-built testing setup composed of a monochromator (Princeton Instrument, SP2150), an oscilloscope (Tektronix, DPO 5104B), and a light source (Energetiq, Eq. (99-)X) was employed. Before device characterization, the intensity of the incident light was calibrated by a powermeter (PM 100D, Thorlabs GmbH.).

3. Results and discussion

Figure 1(a) shows the step-wise device construction process which mainly involves the direct transfer of single layer graphene on the surface of TiO_2 wafer. After graphene transfer, silver paste serving as electrode was placed on both foil and the graphene. For convenience, the as-fabricated UVA and violet PD was then mounted on a printed circuit board (PCB), as shown in Fig. 1(b). The representative top-view SEM image of the graphene-single-crystal TiO_2 interface is displayed in Fig. 1(c). Due to their distinct difference in contrast, both graphene and TiO_2 can be easily visualized in the scanning electron microscopy (SEM) image. Further Raman spectrum of the graphene derived from CVD method was displayed in Fig. 1(d), from which one can observe that there are three obvious peaks in total: two strong peaks at $\sim 1510\text{ cm}^{-1}$ (G-band) and $\sim 2634\text{ cm}^{-1}$ [2D-band, the full width at half maxima (FWHM) is $\sim 56\text{ cm}^{-1}$], and another one at 1346 cm^{-1} (D-band), respectively. The intensity ratio of 2.1 ($I_{2D}:I_G$) and the relatively weak D-band scattering confirms the single layer graphene with some defect in the structure [23, 27].

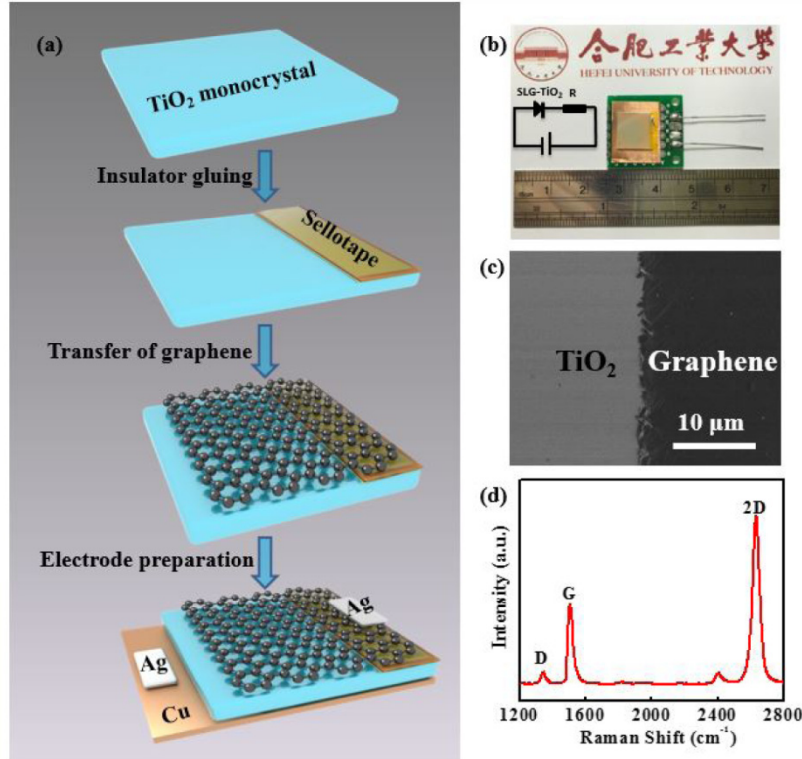


Fig. 1. (a) Flow chart for the fabrication of the p-type graphene-TiO₂ PD. (b) The digital photograph of the PD, the inset shows the equivalent circuit. (c) Top-view SEM image of the graphene-single-crystal TiO₂ interface. (d) Raman spectrum of the SLG film.

The I - V characteristic of the p-type graphene-TiO₂ heterojunction was then studied. As shown in Fig. 2, like conventional metal-semiconductor contact, the current graphene-TiO₂ heterojunction exhibits representative rectifying behavior, with a reverse saturation current of less than $\sim 1.0 \times 10^{-9}$ A. The on/off ratio is estimated to be 10^2 at bias voltage of ± 5 V. Such rectifying characteristic can be ascribed to the SLG-TiO₂ Schottky junction, as indicated by the equivalent circuit (the inset of the Fig. 1(b)). The Schottky barrier height of graphene-TiO₂ (Φ_{ns}) heterojunction was then extracted from the I - V characteristic by using the following equations [28, 29]:

$$J = J_{ST} \left[\exp\left(\frac{qV}{nkT}\right) - 1 \right] \quad (1)$$

$$J_{ST} = A^{*2} T \exp\left(-\frac{q\Phi_{ns}}{kT}\right), A^* = 4\pi q m^* k^2 / h^3 \quad (2)$$

where J is the current density, J_{ST} is the reverse saturation current density, q is the elementary charge, V is the bias voltage, n is the ideality factor ($n = \frac{q}{kT} \frac{dV}{d \ln I}$), k is the Boltzmann

constant, A^* is the Richardson constant, m^* is the effective mass of the charge carriers ($m^* = 0.09m_0$, the rest mass of electrons) [28]. By fitting the above equations, the Φ_{ns} can be calculated to be 0.88 eV. This value is comparable to other graphene-semiconductor contacts such as graphene-ZnO (0.5-1 eV) [19] and graphene-GaAs (0.71 eV) [30].

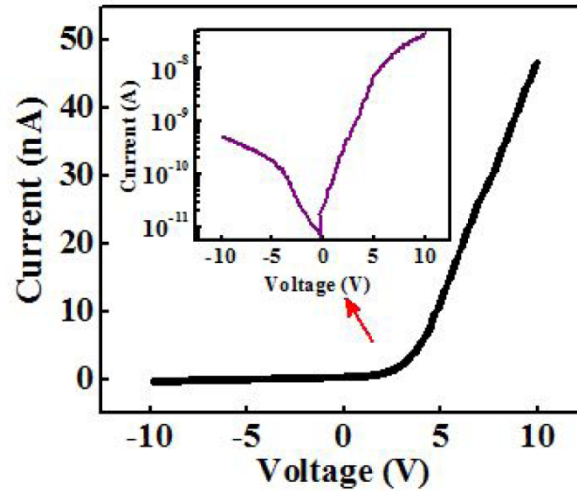


Fig. 2. I - V curve of the SLG-TiO₂ Schottky junction PD in dark, the inset shows the I - V curve on a logarithmic scale.

When the SLG-TiO₂ heterojunction device is shined by ultraviolet light with wavelength of 405 nm, it will exhibit pronounced photoconductivity. Figure 3(a) shows the photoresponse of the device as the incident light was repeatedly turned on and off. It is easy to find that the present device can be readily switched between high- and low- conduction states, with an on/off ratio as high as 10^4 . Notably, such a photosensitivity is highly reproducible and it can retain the nearly identical photocurrent even when the device was stored at ambient condition for 1 month. It should be pointed out that the photosensitivity of our device is highly dependent on the irradiation intensity. Figure 3(b) shows the I - V characteristics of detector under light illumination with various intensities, from which one can see that the photocurrent gradually increases at both reverse and forward bias voltages (reverse bias means the metal electrode is negatively biased, while the forward bias means the metal electrode is positively biased). What is more, at all light intensity, the sensitivity is very stable and reproducible [Fig. 3(c)]. As a matter of fact, the above light intensity dependent photocurrent can be described by a power law: $I = AP^\theta$, where I , A , P and the exponent θ denote the photocurrent of PD, the constant for a certain wavelength, the incident light intensity, the exponent which determines the response of photocurrent to light intensity, respectively [31]. By fitting the I - P curve in Fig. 3(d), θ was estimated to be 0.57. Such a relatively low value confirms the presence of defects species in the PD, as indicated by the Raman analysis in [Fig. 1(d)]. Finally, it is also revealed that the on/off ratio of the PD increase gradually which increase with increasing light intensity [Fig. 3(e)]. The on/off ratio is as high as 6.8×10^4 when the light intensity reaches 65 mW/cm^2 . This on/off ratio is relatively higher than that of other TiO₂ based photodetectors.

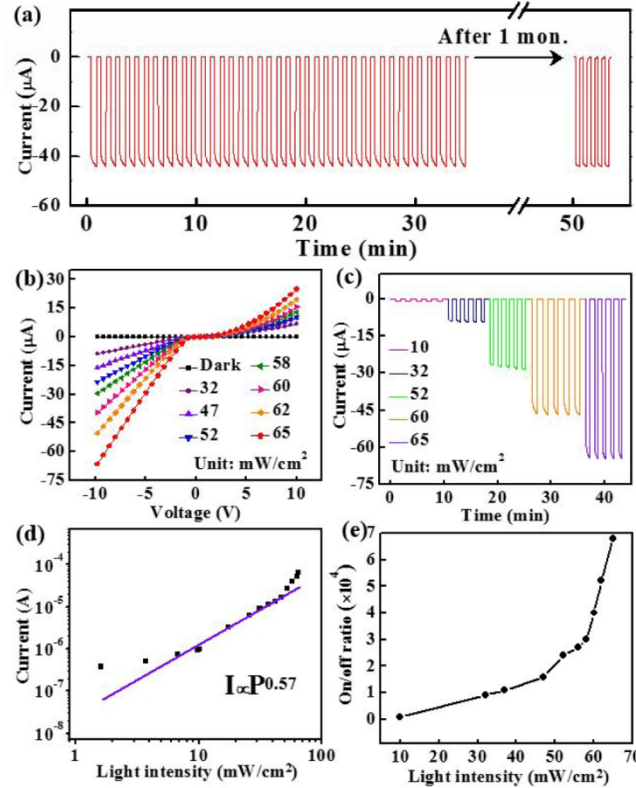


Fig. 3. (a) Photoresponse of the device at 10 V reverse bias under 40 cycles with light illumination of 60 mW/cm² before and after 1 month. (b) I - V curves of the device under different light intensities. (c) Photoresponse behavior of the device under light with different light intensities, this measurement was carried out at a bias voltage of -10 V. (d) The fitting of the relationship between the photocurrent and light intensity, $\lambda = 405$ nm. (e) The relationship between on/off ratio of the device and light intensity at 10 V reverse bias.

To quantitatively assess the device performance of the present SLG-TiO₂ PD, two key parameters, responsivity (R) and detectivity (D^*) that denote the photodetector sensitivity to incident light were calculated by using the following equations [32, 33]:

$$R(AW^{-1}) = \frac{I_p - I_d}{P_{opt}} \quad (3)$$

$$D^* = \sqrt{\frac{A}{2qI_d}} R \quad (4)$$

where I_p represents the photo-excited current under light illumination, I_d the current without light illumination, P_{opt} the power of the incident light, h the Planck's constant, q the elementary charge, and A the active area of the PD (0.64 cm²), respectively. Figure 4(a) further plots the relationship between R , D^* and light intensity. Similar to the evolution of the on/off ratio, both R and D^* shows similar tendency. That is, both R and D^* increase when the light intensity increases from 10 to 65 mW/cm². According to the above equations, the photoelectric responsivity, normalized detectivity under the light power of 65 mW/cm² are calculated to be 1.63 mA W⁻¹ and 7.29×10^{10} cm Hz^{1/2} W⁻¹, respectively. It is also revealed that photocurrent of the PD is also highly dependent on the bias voltage [Fig. 4(b)]. Figure 4(c) plots the photocurrent as a function of bias voltage. Apparently, the photocurrent

increase gradually with increasing bias voltage. According to previous study, this finding can be ascribed to increased drift velocity of photoexcited charge carriers and suppressed recombination activity at high bias voltage [34, 35].

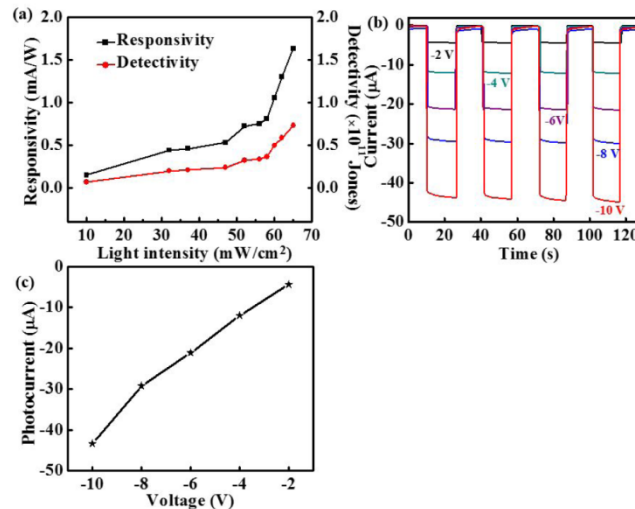


Fig. 4. (a) Responsivity and detectivity as a function of the light power at -10 V bias. (b) Photoresponse behavior of the device at various reverse bias voltages under light illumination of 60 mW/cm^2 . (c) The relationship between photocurrent and reverse bias voltages of the PD.

In addition to light intensity and bias voltage, the photocurrent of the PD is dependent on wavelength of the incident light as well. Figure 5 shows the spectral photoresponse of the device in the range from 300 to 600 nm (The light intensity was calibrated and kept identical during the spectra response analysis so as to make the data more reliable). It can be seen that the photocurrent of the PD is relatively low when under light illumination with wavelength of either less than 330 nm, or longer than 490 nm, suggesting the PD is nearly blind to the illumination in the above region. Nonetheless, once the device is shined by light in the range between 330 and 490 nm, the sensitivity increases steeply and reaches a maximum at 410 nm. Notably, the FWHM is estimated to be 82 nm (from 368 to 450 nm), which means this device has a relatively narrow spectral response. Such a spectral selectivity is actually in good agreement with the absorption spectra, which shows strong absorption in the same range. Understandably, such a spectral response is associated with its photoelectric mechanism. When the PD is irradiated with light, photons with wavelength of 410 nm (E_{g, TiO_2} : 3.2 eV) have sufficient energy to lift electrons in the TiO_2 from the valence band to the conduction band. As a result, photo current is formed in the circuit. The slight drop on the shorter wavelength (wavelength less than 330 nm) is related to the enhanced absorption of high-energy photons at or near the surface region of the TiO_2 wafer. In this case, the electron-holes generated near the surface region has a relatively shorter lifetime than those in the bulk, thus, they contribute less to the photocurrent [36].

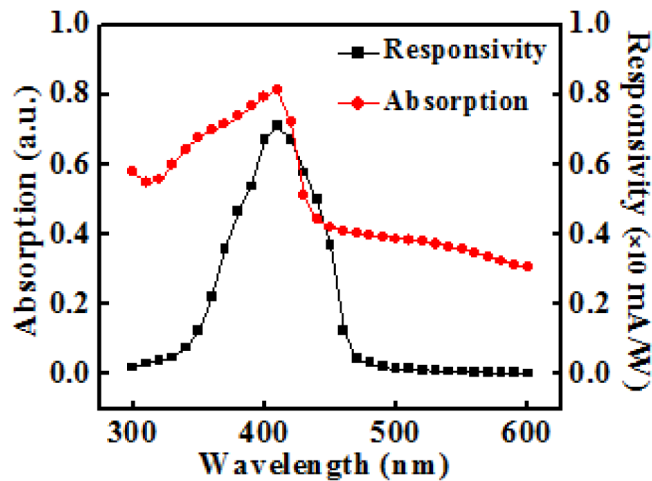


Fig. 5. Spectral response and absorption spectrum of the PD.

To further study the potential for detecting fast optical signal, the optoelectronic property of PD under illumination of fast-switching light was studied [Fig. 6(a)]. Figures 6(b)-6(g) depict the photoresponse of the SLG-TiO₂ PD to pulsed light irradiation with frequency of 5 Hz, 10 Hz, 50 Hz, 100 Hz, 200 Hz, and 400 Hz, respectively. It can be seen that the SLG-TiO₂ Schottky junction PD could be readily switched between off- and on-state with good reproducibility. Further relative balance as a function of varied frequency shows that the device has a slow relative balance $[I_{\max}-I_{\min}/I_{\max}]$ decay. As shown in Fig. 6(h), the relative balance of the PD is still larger than 70% even though the frequency is as high as 400 Hz. By fitting a single normalized cycle of photoresponse under 400 Hz light illumination plotted in Fig. 6(i), the response time or rise time τ_r (defined as the time required for the photocurrent to increase from 10% to 90%) and the recovery time or decay time τ_f (defined analogously) for the p-type SLG-TiO₂ PD were determined to be 0.74 and 1.18 ms, respectively. Considering the rise/fall time is limited by the RC time constant of the device, the above rise/fall time can be further fastened by reducing the area or thickness of TiO₂. To directly compare the performance of our PD with other TiO₂ based devices, some key metrics such as responsivity, detectivity, response time, and on/off ratio are summarized in Table 1, from which one can learn that although the responsivity is relatively poor, our device shows obvious advantages in on/off ratio, which is high as 6.8×10^4 , the best among the all the TiO₂ based devices. What is more, the τ_r/τ_f have the lowest values, which means that the response speed of the present SLG-TiO₂ PD is much faster than not only the PDs based on individual TiO₂ nanotube and nanorods, but also than other TiO₂ based heterojunction including TiO₂-poly (9, 9-dihexylfluorene) (PFH) composite, Au/TiO₂ thin film/Au, Ag/TiO₂ nanotube array /fluorine-doped (FTO) Schottky junction PDs. Without doubt, such a fast response speed due to the high-quality Schottky junction [37], along with the high on/off ratio and easy fabrication process renders the current PD highly promising building blocks for fabricating high-performance optoelectronic system in the future.

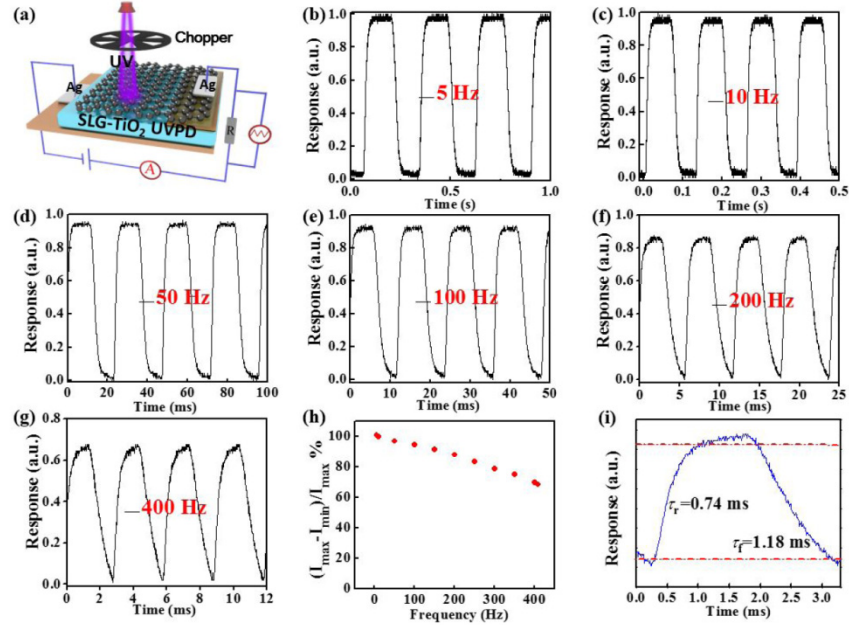


Fig. 6. (a) Illustration of the setup for measuring the response speed of PD. Photoresponse of the device to switchable light illumination (wavelength: 405 nm) with a frequency of 5 Hz (b), 10 Hz (c), 50 Hz (d), 100 Hz (e), 200 Hz (f), 400 Hz (g), respectively. (h) The relative balance $(I_{\max} - I_{\min})/I_{\max}$ versus switching frequency. (i) A single normalized cycle measured at 400 Hz for determining both rise time (τ_r) and fall time (τ_f).

Table 1. Comparison of the PD performance with other TiO₂ nanostructures based devices.

Device structure	Responsivity (A/W)	τ_r/τ_f (ms)	On/off ratio	Ref.
SLG-TiO ₂ heterojunction	0.0016	0.74/1.18	6.8×10^3	This work
Single TiO ₂ nanotube	/	390/450	1.6	[3]
TiO ₂ nanocrystals/PFH structure	0.0546	<200/5000	10^3	[4]
Ag/TiO ₂ nanotube arrays/FTO	176.3	82000/14000	1.073×10^4	[5]
Au/TiO ₂ thin film/Au	199	6000/15000	~45	[6]
TiO ₂ nanorods arrays	0.025	150/50	~50	[10]

The working mechanism of the present SLG-TiO₂ Schottky junction PD can be interpreted by the energy band diagram illustrated in Fig. 7. The intrinsic TiO₂ wafer shows a weak *n*-type electrical property due to defect species, while the HNO₃ treated graphene exhibits typical p-type conductivity [38]. When both materials are brought into contact, owing to their difference in work function, the electrons in TiO₂ will move to the SLG side. As a consequence, a space charge region (also termed as built-in electric field) with a direction pointing from the TiO₂ to graphene film will be intermediately formed. When shined by incident light, the photo-generated electron and holes could be separated by the electric field in the opposite direction, in other words, the holes will move to the graphene side while the electrons diffuse into the TiO₂ side, giving rise to photocurrent in external circuit. During this photoelectric process, only photons with energy larger than the bandgap of TiO₂ can be absorbed, and form effective photocurrent in the circuit. Photons with less energy may be absorbed by the TiO₂, but the absorbed photons are unable to generate photoexcited electron-

hole pairs due to their insufficient energy. Therefore, these photons cannot contribute to the photocurrent in circuit.

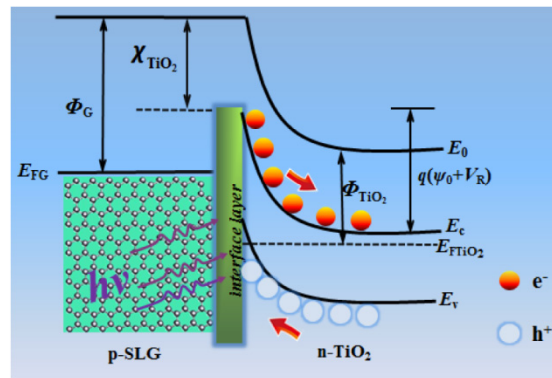


Fig. 7. Energy band diagram of the PD with light illumination at a reverse bias. Φ and EF are the work function and Fermi energy level of the single crystal TiO_2 or SLG film, respectively, χ_{TiO_2} represents the electron affinity of TiO_2 , E_v and E_c are the valence band and conduction band of TiO_2 , respectively.

4. Conclusions

In summary, we presented a simple Schottky junction PD by transferring SLG film onto the surface of rutile single-crystal TiO_2 for UVA and violet light detection. Optoelectronic analysis reveals that the photocurrent of the PD depend on both light intensity and light wavelength. The responsivity, detectivity and on/off ratio of the device were calculated to be 0.0016 A/W , $7.29 \times 10^{10} \text{ cmHz}^{1/2}\text{W}^{-1}$, and 6.8×10^4 at the light power of 65 mW/cm^2 , respectively. In addition, the device was able to probe fast-switching optical signal with frequency as high as 400 Hz with very good reproducibility. The rise/fall times were estimated to be 0.74 and 1.18 ms , which are far faster than most other TiO_2 based devices. The study indicates the present SLG- TiO_2 PDs are promising building blocks for constructing high-speed, high-sensitivity UV optoelectronic nanodevices.

Funding

National Science Foundation of China (NSFC) (21501038, 61575059, 61675062); the Fundamental Research Funds for the Central Universities (2012HGCH0003, 2013HGCH0012, 2014HGCH0005); the Natural Science Foundation of Anhui Province (1408085ME90).